An investigation on Oxidation/Carburisation of 9Cr-1Mo Steel Heat Exchanger Tube in an AGR Environment

Sabrina Yan, Scott Doak, Rachel Thomson and Rebecca Higginson

Materials Department, Loughborough University, Loughborough, Leicestershire, LE11 3TU, UK

Abstract

9Cr-1Mo steels have been used extensively in the power generation industry. In this study, a wide range of experimental samples exposed at different times and temperatures in a CO_2 environment were analysed to look at the development of the metal and oxides over time. The main objective of this work was to obtain a better understanding of the carburisation and oxidation behaviour of 9Cr 1Mo steels as a function of temperature/time, with special attention paid to the transition from protective to breakaway oxidation. In addition, experiments were also carried out to investigate any links between oxidation transition and carburisation behaviour of these materials.

Keywords: carburisation, oxidation, oxide scale, 9Cr-1Mo steels, characterisation

1. Introduction

9Cr-1Mo steels have been used in conventional and nuclear power generation due to their mechanical properties and resistance to the harsh environments. After long term service in power plant, a dual-layered oxide scale structure is developed which consists of a coarse grained outer oxide (magnetite) and a fine grained inner oxide (mixed oxide spinel). A transition of oxidation has been observed in previous studies [1-3], from protective oxidation to breakaway oxidation, where there is a rapid increase in the growth rate of oxide scale which leads to oxide scale spallation and metal loss.

Studies have been carried out to look at the oxidation behaviour of similar steels [1-4], and it has been shown that the breakaway oxidation is not only a result of oxidation but could also be affected by the process of carburisation, which is a continued diffusion process of carbon from the metal oxide interface into the substrate maintained as a carbon activity gradient by the precipitation of Cr rich carbides [1]. An accumulation of carbon appears at the magnetite/Fe-Cr spinel oxide interface [4] and the amount of carbon up-take is approximately proportional to the extent of oxidation [1]. Breakaway oxidation or non-protective oxidation is found to be associated with the establishment of a critical carbon concentration at the metal/oxide interface [1-2].

In this study, systematic experiments have been carried out on a set of finned tube samples, which have been tested in an autoclave by AMEC Foster Wheeler to simulate power plant conditions in terms of service temperatures, gas/moisture conditions and pressures. Carbon concentration measurements were collected at different locations across the fin of a set of samples. A detailed carbide study of size distribution across the fin and chemistry distribution within carbides was also carried out. Chemical analysis at different locations across the dual-layer structured oxide scale at different stages of oxidation of the fins (pre-breakaway and post-breakaway) was carried out.

2. Experimental Procedure

2.1 Materials and sample preparation

A set of experimental samples of finned tube was selected with different heat treatment history; details of gas/moisture conditions, pressure, temperatures and duration time are tabulated in Table 1. The nominal composition and a reference

composition of P91 type of steel are listed in Table 2. All samples were cross-sectioned and mounted in conductive bakelite for microscopic analysis.

Table 1 Table of heat treatment conditions of samples examined in this study.

Sample ID	*Gas Condition (vppm)*	*Pressure (psig)*	*Temperature (°C)*	*Duration (hours)*	*Breakaway*
HRA virgin	*-*	*-*	*-*	*-*	*-*
HRA 8525	*400*	*600*	*600*	*5845*	*N*
HRA 8526	*400*	*600*	*600*	*10865*	*Y*
HRA 8556	*400*	*600*	*600*	*19924*	*Y*
HRA 8575	*400*	*600*	*600*	*25962*	*Y*

Table 2 The nominal chemical compositions of the as-received materials in weight %. The ASTM P91 standard [5] specifies the minimum and maximum concentrations.

Element	*As-received sample*	*ASTM P91*		
		Average	*Min*	*Max*
C	*0.093*	*0.10*	*0.08*	*0.12*
Cr	*9.2*	*8.75*	*8.0*	*9.5*
Mo	*1.04*	*0.95*	*0.85*	*1.05*
Si	*0.67*	*0.35*	*0.20*	*0.50*
Mn	*0.47*	*0.45*	*0.30*	*0.60*
P	*0.011*	*0.01*		*0.02*
Ni	*0.21*	*0.2*		*0.4*
Co	*0.02*			
Cu	*0.16*			
Nb	*< 0.02*	*0.08*	*0.06*	*0.10*
Ti	*< 0.02*	*0.005*		*0.01*
V	*< 0.05*	*0.22*	*0.18*	*0.25*
W	*< 0.05*			
N		*0.05*	*0.03*	*0.07*
Al		*0.01*		*0.02*
Zr		*0.005*		*0.01*

For the microstructural analysis undertaken, a high standard of sample preparation was required. All samples were prepared with extended polishing steps to minimise grain pull-out in the oxide layers and metal matrix. A final colloidal silica polishing step was used so that the samples had a deformation-free surface (0.04 μm surface finishing). A Hitachi ZoneSEM cleaner was used to clean the samples using a 30

minute cleaning procedure with the minimum pressure value setting (highest cleaning intensity) to remove surface hydro-carbons before carbon content measurements were carried out.

2.2 Analytical procedures

A number of electron microscopes were used in this work to carry out analytical experiments. Carbon content measurements were conducted using a field emission scanning electron microscope (JEOL 7100F FE-SEM) equipped with an energy dispersive spectrometer (EDAX Octane 60 mm). An accurate probe current value was available during carbon measurement from the probe current detector installed onto this system. Carbon contents were measured and calibrated using net peak intensity of carbon per probe current [6].

Quantitative analysis of carbide particles was carried out using ion induced secondary electron images, which were collected from a FEI Nova 600 Nanolab dualbeam system. A XeF_2 reactive gas was used to suppress ion channeling contrast with a probe current of 0.5 nA and a frame time of 47.6 s. A horizontal field width of 50 µm was chosen for each image and the stage was moved in 50 µm increments so that a continuous line of images containing the particles was collected. Figure 1 shows the positions where those images were collected from. The particles in the images were quantified using a threshold based binarisation method using ImageJ software [7].This dualbeam system was also used to prepare site-specific TEM samples using an in situ lift-out approach [7].

In general, all lamellae were approximatedly 15 µm x 5 µm and prepared from three different locations in the middle fin as shown in Figure 1. The lifted out samples were attached to the chevron in the support grid so that the area to be thinned to electron

transparency could be chosen. A FEI Tecnai F20 Field Emission Transmission Electron Microscope (FE-TEM) was used to examine these lamellae. The system is equipped with a windowless X-max 80 Silicon Drift Detector (SDD) Energy Dispersive Spectroscopy (EDS) system for elemental analysis. This system was used primarily for chemical mapping using Aztec software. Spectrum maps were collected using high current settings to ensure a good signal to noise ratio. The chemical identity of features of interest was analysed by post-collection processing.

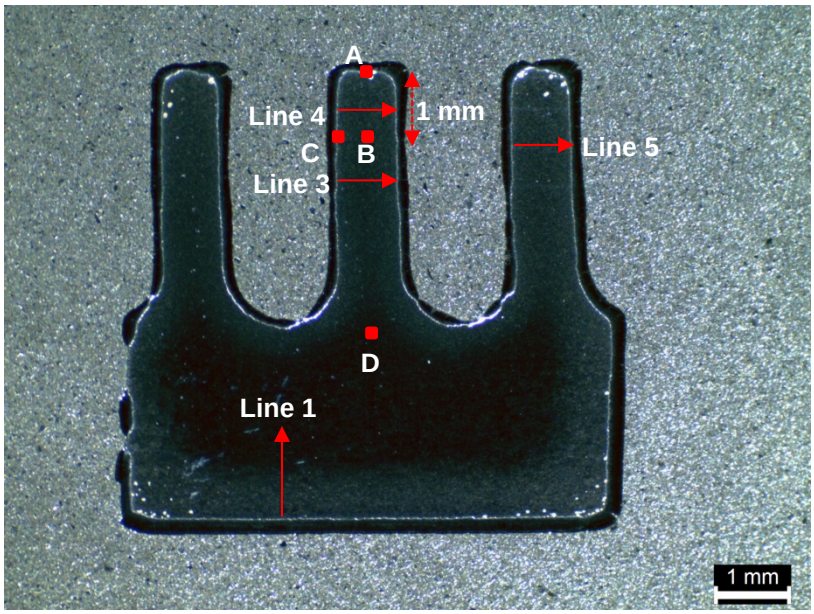

Figure 1 Optical micrograph of a typical experimental sample finned tube cross section, showing three locations where TEM lamellae were prepared, labelled by red spots as A—fin tip location, B—mid fin location, C—fin edge location and D—baseline location respectively. In addition, four locations where the carbon content measurements and carbide particle analysis were carried out, labelled by solid red arrow lines as Line 1—from base to bulk of tube, Line 3, 4 and 5—across the fin from left side to right side of metal/oxide interface.

3. Results and Discussion

General overview

Optical images of samples examined in this study are shown in Figure 2. Oxide scales on these samples are clearly visible in these micrographs and in general the oxide scale thickness increases with exposure time. Oxide scales at the fin tips are

generally thicker than other locations around the samples. Cracks are likely to be initiated at the fin tip corners as shown in Figure 2 (c-d) by red circles. Post-breakaway samples showed rapid oxide scale growth and then fin material loss (Figure 2 (d and e)).

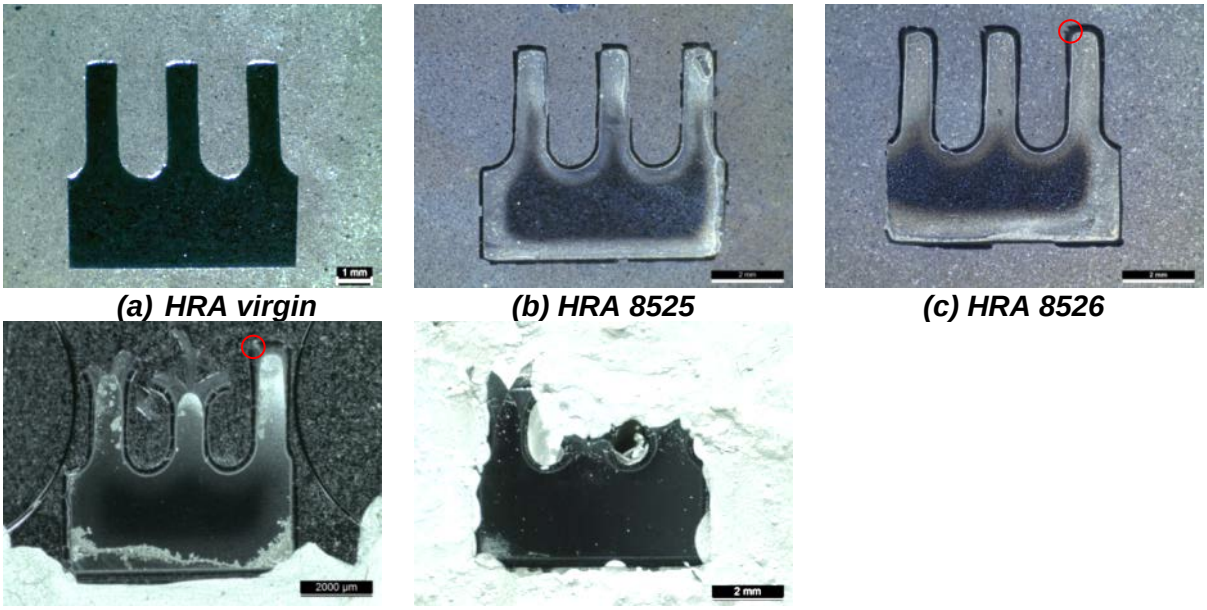

(a) HRA virgin ***(b) HRA 8525*** ***(c) HRA 8526***

(d) HRA 8556 ***(e) HRA 8575***

Figure 2 Optical images showing the cross sections of the five samples, (a) HRA virgin sample, (b) HRA 8525, (c) HRA 8526, (d) HRA 8556 and (e) HRA 8575.

Carbon content measurements

Carbon profiles are presented in Figure 3 for samples HRA 8556 and HRA 8575. A consistent overall trend was observed from all line 1 scans (see Figure 1) in the samples: the carbon level peaked at the oxide/metal interface and decreased in an approximately linear manner from the interface towards the centre of the sample. The carbon content approached a steady level around 400 µm away from the oxide/metal interface (as shown in Figure 3 (a)). The breakaway sample (HRA 8575) showed a slightly higher carbon content across the profile line 1 location and approached a steady level around 800 µm away from the oxide/metal interface

(Figure 3 (c)). The increase in carbon content in the fin bulk serves as evidence of carbon diffusion during exposure.

All fin location measurements (lines 3, 4 and 5) showed a similar trend of the carbon content variation across the fins with carbon level trend across the fins looks like a ‘V’ or ‘U’ shape, it decreased from the oxide/metal interface at both the left and right side fin edges and reached the lowest point at the middle of the fin (Figure 3 (b)). However, the carbon content was found to be different around the fins at different locations. All line 4 scans showed a slightly flatter trend compared with lines 3 and 5. This trend suggests that as the measurements approach the fin tip, carbon content level became more homogeneous across the fin. The reason for this was as you approach the fin tip, the proximity to a free surface was higher, hence more carbon was absorbed not only from the oxides at the fin edge but also the fin tip.

Carbide particles analysis

A series of ion induced secondary electron images were collected from the samples across the middle fins at different locations (as indicated in Figure 1), in order to obtain a visual comparison of the carbide particles size/area fraction between different locations across the fin. Three representative images are selected from each line (lines 3 and 4 in Figure 1) at the oxide/metal interface and the middle of the fin respectively. These micrographs are shown in Figure 4 and Figure 5 from the HRA virgin sample and the HRA 8526 sample respectively.

Carbide particles were observed in the HRA virgin sample mid fin (Figure 4) and they were found to have a relatively homogeneous distribution at the selected locations. Carbide particles were mainly globular shaped, and a few special ‘ring’ (with matrix

in the core) shaped ones observed as highlighted in red circles in Figure 4. Carbides were found to be formed both intergranularly and intragranularly.

The HRA 8526 sample was determined as a sample experiencing breakaway oxidation, with the carbide particles found to be coarsening in size (Figure 5). Carbide particles across this sample at positions 3 and 4 showed slightly different distributions in the middle of the fin. The middle of the fin at position 3 showed less carbide particles compared to other locations. Two types of carbide particles were observed in terms of their different morphologies, blocky carbides and fine needle shaped type of carbides. Those larger carbides were most likely found to be segregated on grain boundaries and the fine needle shaped type carbides were found in all locations, mainly intragranularly distributed.

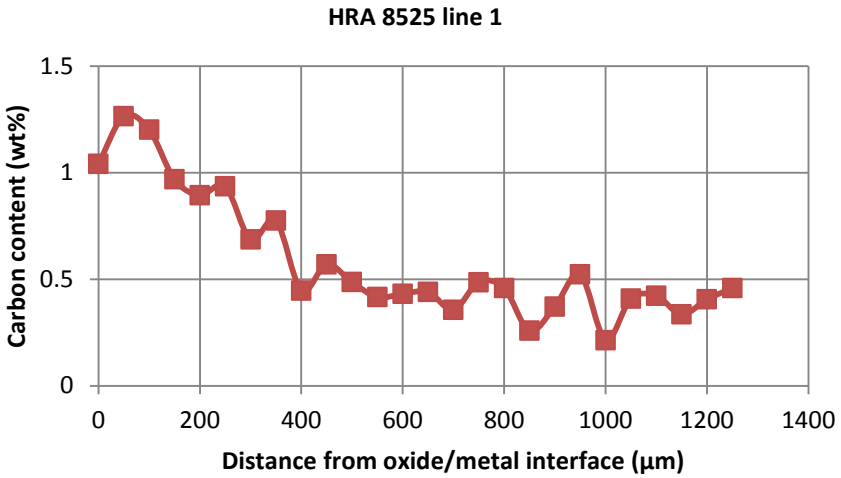

(a)

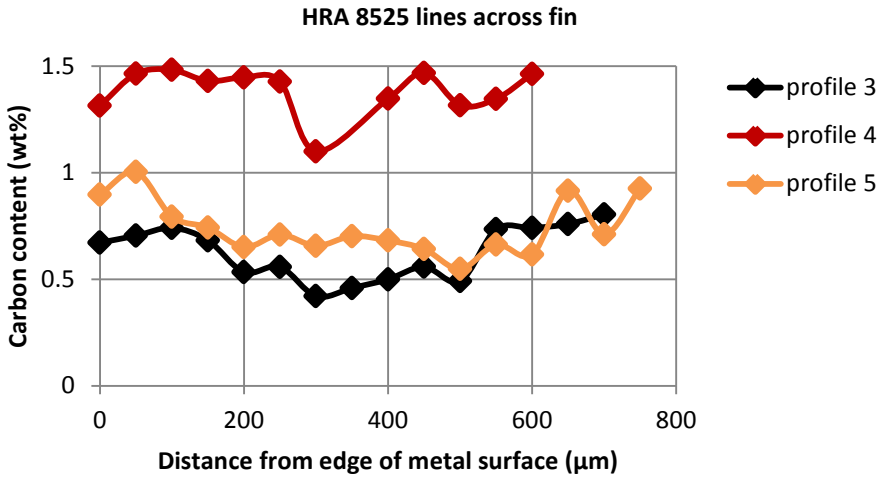

(b)

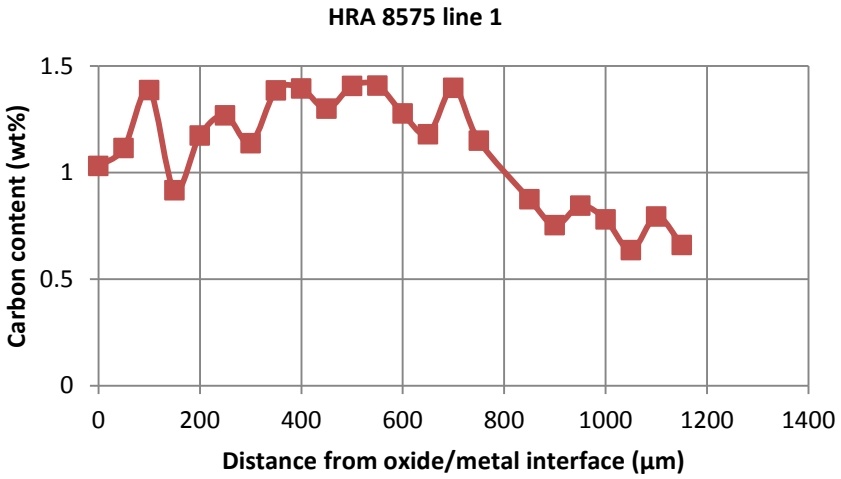

(c)

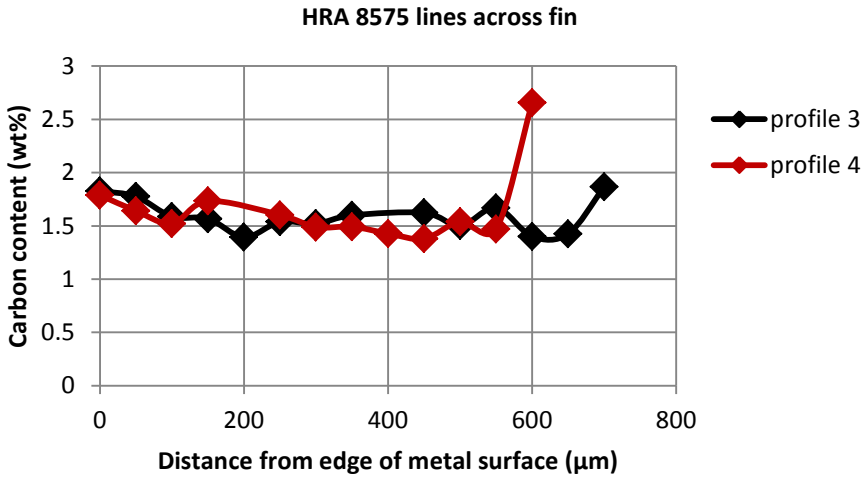

(d)

Figure 3 Calibrated carbon concentration line profiles of samples HRA 8525 and HRA 8575 at different locations as shown in Figure 1.

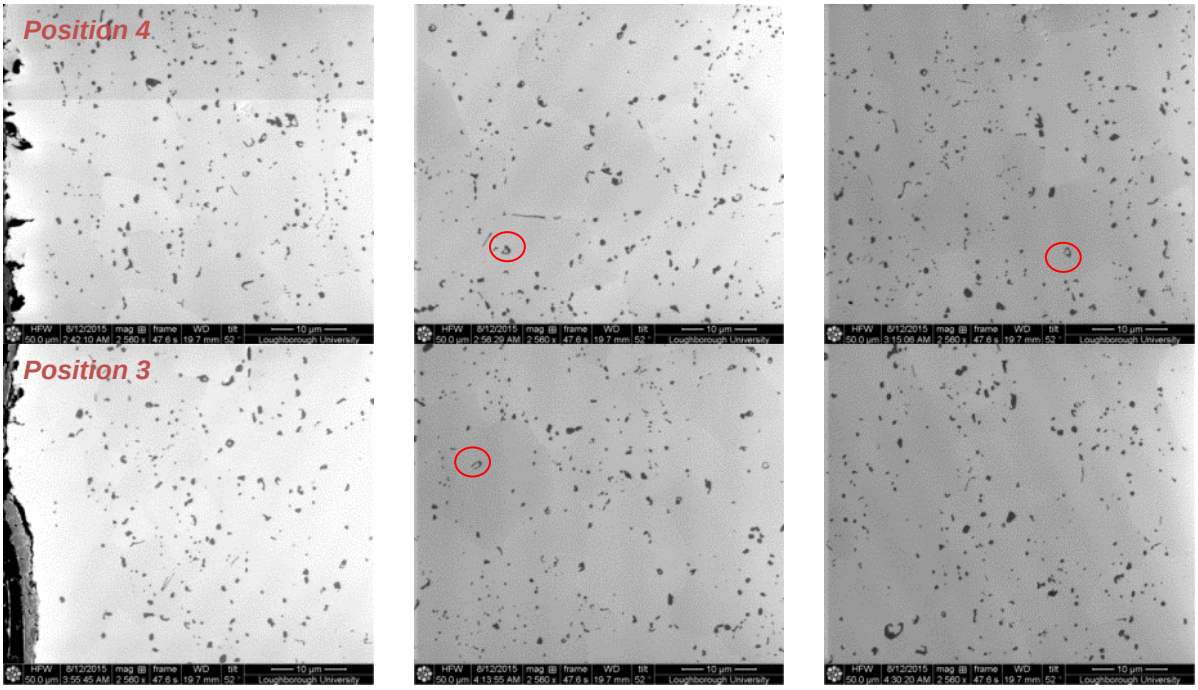

Figure 4 Ion induced secondary electron images collected from two locations (labelled as position 3 to 4) on the middle fin of sample HRA virgin. Three images per location were presented from left to right in each column left side fin edge at oxide/metal interface, middle point across the fin and right side fin edge at oxide/metal interface.

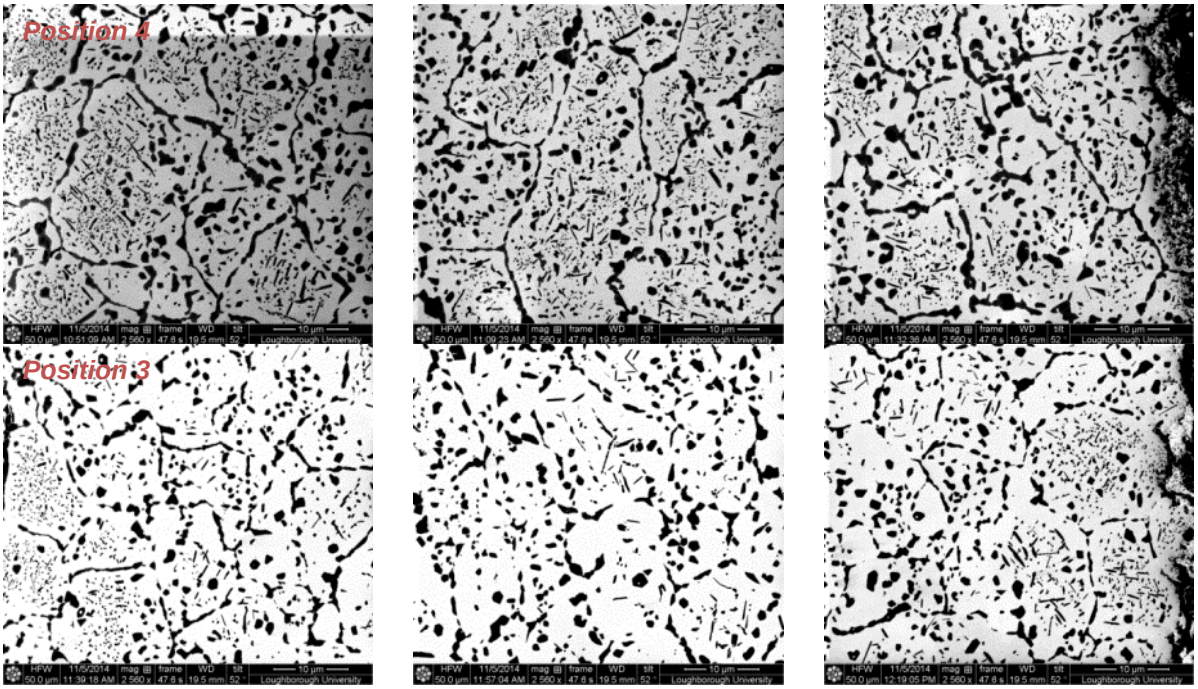

Figure 5 Ion induced secondary electron images collected from two locations (labelled as position 3 to 4) on the middle fin of the sample HRA 8526. Three images of each location were presented from left to right in each column: left side fin edge at oxide/metal interface, middle point across the fin and right side fin edge at oxide/metal interface.

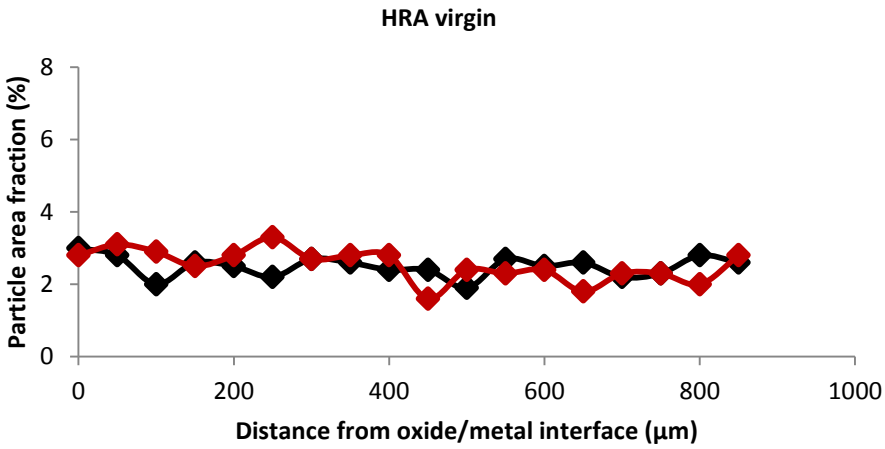

(a)

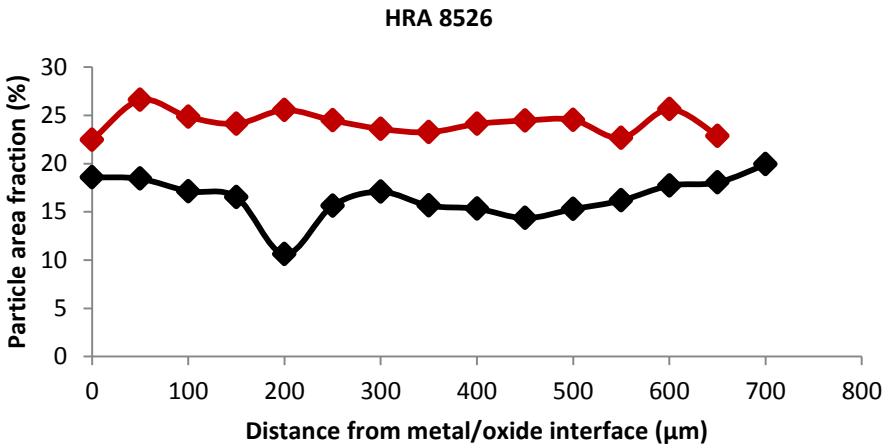

(b)

Figure 6 Plots of carbide particles area fraction per unit area across fin of (a) HRA virgin sample and (b) sample HRA 8526. Black line—position 3 and red line—position 4.

Carbide particle area fractions across the locations 3 and 4 of each sample were obtained and Figure 6 shows a comparision of carbide particles area fraction across locations 3 and 4 between HRA virgin sample and HRA 8526 sample. The HRA virgin sample plot (Figure 6 (a)) showed that the carbides were evenly distributed across location 3 and 4 in the mid fin, which is consistent with the visual examination of ion induced secondary electron images.

After longer term exposure, carbides were found to be distributed more evenly across the fins at different locations as indicated by the flat area fraction across the

fins in Figure 6 (b). In sample HRA 8526, carbide area fraction across location 4 was found to be much higher than the other locations.

A summary of quantitative maximum and minimum area fraction at each location of two selected samples is given in Table 3. Area fractions of carbides at location 3, 4 and 5 of both HRA virgin sample and HRA 8526 breakaway sample are tabulated. The area fraction values collected from the as-received sample showed the same results as visual inspection of the previous ion induced secondary electron images. The area fraction of carbide particles of sample HRA 8526 is much higher than the HRA virgin sample especially towards the fin tip location.

Table 3 Summary of carbide particle area fraction of HRA sample set at three locations (3, 4, and 5) with key exposure conditions.

Sample ID	***Exposure time (hour)***	***Location***	***Area Fraction per unit area (%)***	
			Max.	***Min.***
HRA virgin	*0*	*3*	*3*	*2*
		4	*3.3*	*1.6*
HRA 8526	*19924*	*3*	*19.9*	*10.6*
		4	*26.6*	*22.5*
		5	*19.9*	*13.8*

It has been shown that before breakaway oxidation occurs, both the C content and carbide area fraction decrease in an approximately linear manner from the metal oxide interface towards the centre of the fins, and the amount of C measured near the fin edge was found to be much higher than its nominal composition. This was also reported in previous studies by Rowland and others [2, 3 and 8]: the carbon is being introduced to the alloy as the CO/CO_2 species breaks down at the oxide/metal interface to release oxygen.

The amount of the carbon up take can be correlated to the carbon measurements. The size of the carbides is also found to decrease from the oxide interface to the centre of the sample. This can be explained as the amount of carbon available at the oxide/metal interface is high, which allows larger and more carbide particles to form.

In the fin locations of breakaway samples (HRA 8556/8575), there is no variation in the C content or the area fraction of carbides observed across the fin. However, a higher carbide area fraction was observed in the fin exhibiting breakaway oxidation compare to the pre-breakaway fin.

Oxide scale analysis

Two TEM lamellae were prepared from sample HRA 8556 fin tips, one from the mid fin which experienced breakaway oxidation and the other from the right fin which had yet to experience breakaway (see Figure 2 (d)). A detailed TEM chemical analysis was carried out on these two samples and the results are illustrated in Figure 7 and Figure 8.

In the mid fin tip (breakaway fin tip), two different composition carbide particles were observed and they are a Cr-rich type and a Mo-rich type. Both of these types of carbides possess an average size of 2-3 μm. From the chemical distribution maps in Figure 7, Cr-rich carbides and Mo-rich carbides are joining together and forming a continuous layer at the oxide/metal interface. In the right fin tip (pre-breakaway fin tip), Cr-rich and Mo-rich carbide particles were also observed, with a smaller particle size compared to those found in the breakaway fin tip. However, in this case, a continuous layer of carbide is not formed at the oxide/metal interface. The C distribution maps collected from both breakaway and pre-breakaway fins showed the presence of graphite and this was confirmed by high-resolution TEM image and d-

spacing measurements. From the chemical analysis carried out on the two lamellae, the main difference between these two fin tips was the carbide particle size.

A further 5 TEM lamellae were prepared from the breakaway fin of sample HRA 8556 (Figure 9) and detailed chemical analysis was carried out on all 5 samples. Representative results collected from oxide/metal interface, inner spinel oxide scale and magnetite/spinel interface are shown in Figure 10, Figure 11 and Figure 12 respectively.

At the oxide/metal interface (see Figure 10), the carbides are not as big as those observed at the fin tip location. The same two types of carbides are still visible as at the fin tip. Carbon is found to segregate as “tiger mark” patterns which are found to be enriched in carbon near the spinel/magnetite interface, as shown in C distribution maps in Figure 11 and Figure 12. High-resolution TEM images were collected from these patterns and a representative image was shown in Figure 13, d-spacing measurements suggested that these patterns are mostly likely to be graphite. This observation is consistent with a previous study [9], which claimed that carbon was observed to partition into the inner spinel layer. Several researchers believed that a critical level of carbon in the spinel [2, 3] is critical to the cause of breakaway.

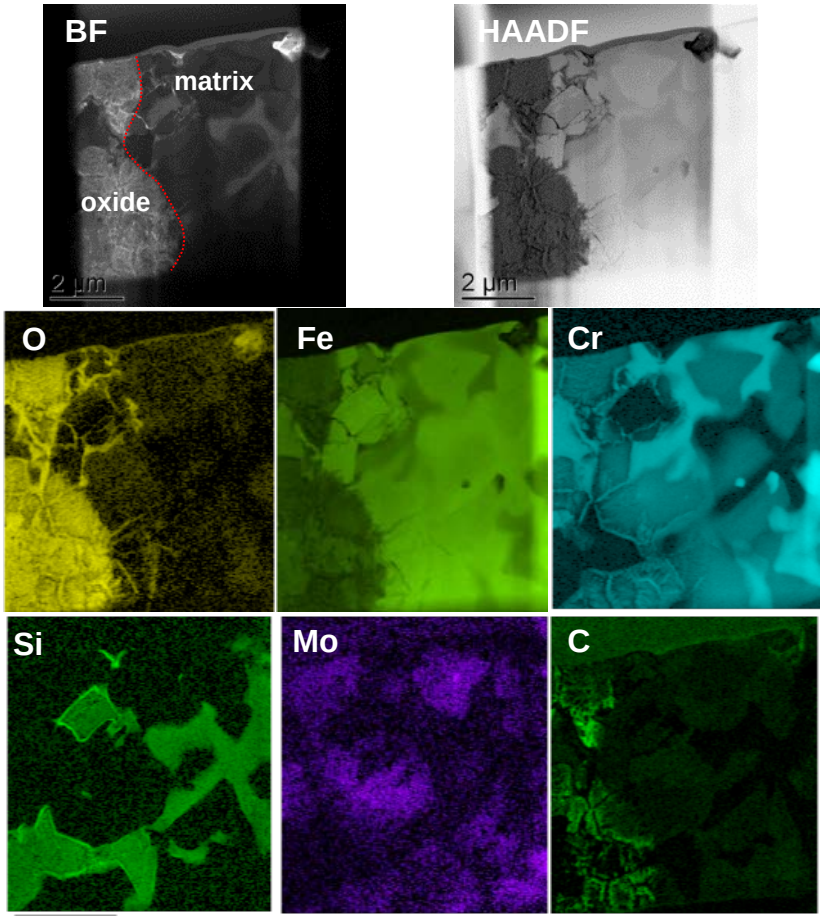

Figure 7 TEM BF and HAADF images with a set of elemental distribution maps collected from the mid fin tip from sample HRA 8556, the oxide/metal interface is highlighted as red dash line.

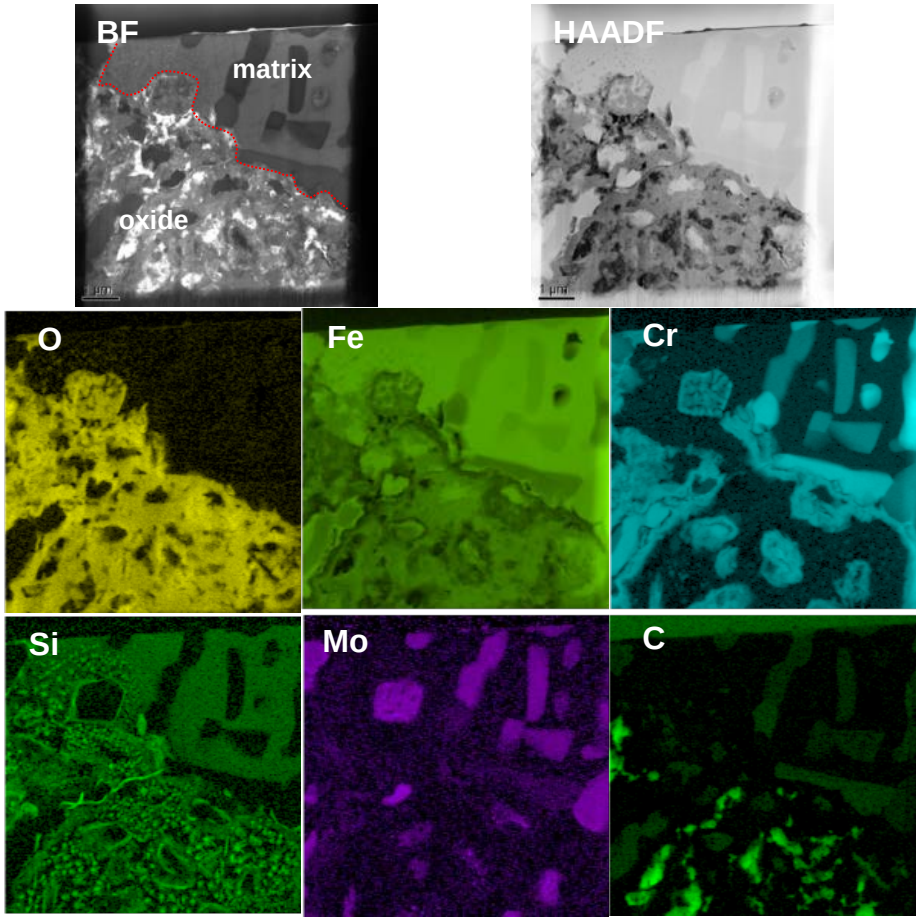

Figure 8 TEM BF and HAADF images with a set of elemental distribution maps collected from the right fin tip from sample HRA 8556, the oxide/metal interface is highlighted as red dash line.

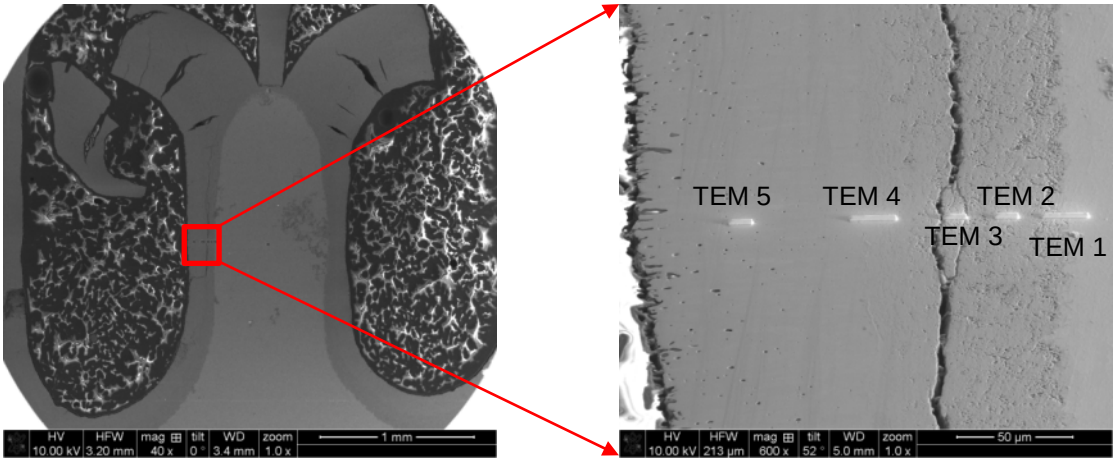

Figure 9 (a) secondary electron image at low magnification showing an overview of the breakaway fin of sample HRA 8556, (b) secondary electron images at higher magnification showing where TEM lamellae were prepared from the mid fin oxide scale of sample HRA 8556.

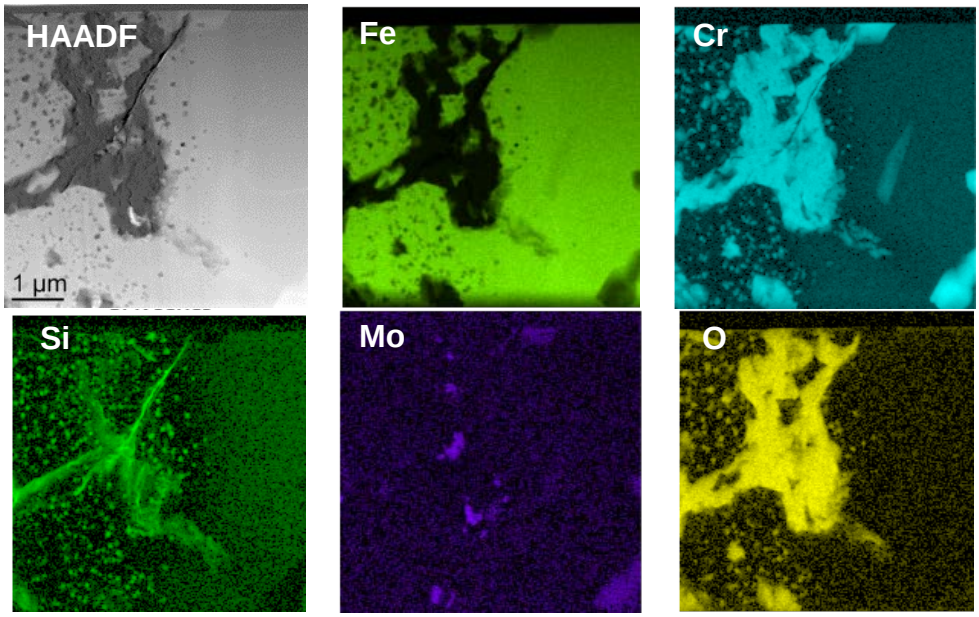

Figure 10 TEM HAADF image with a set of elemental distribution maps collected from the mid fin metal/oxide interface (TEM 1 in Figure 9) from sample HRA 8556.

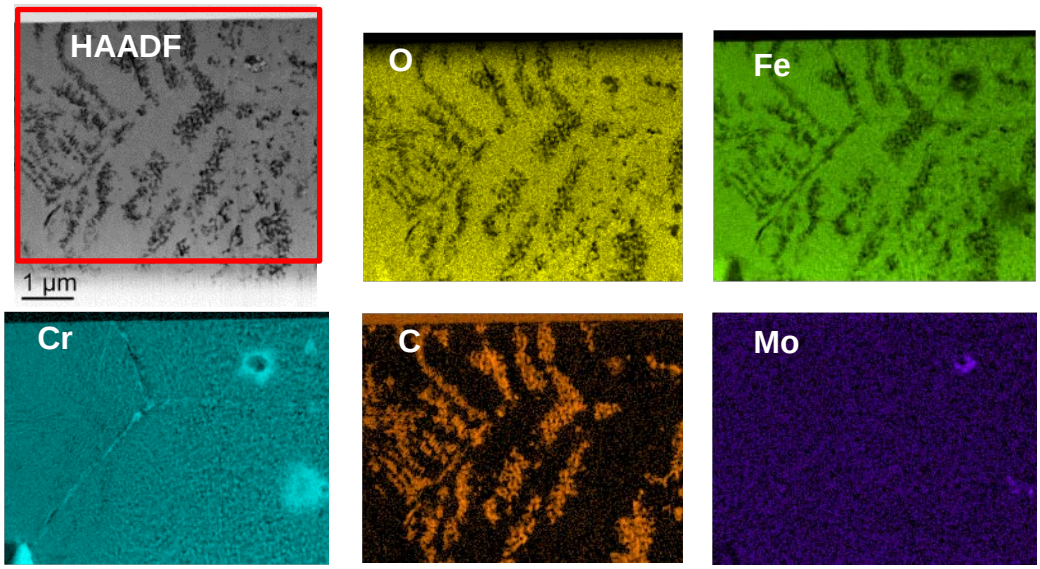

Figure 11 TEM HAADF image with a set of elemental distribution maps collected from the mid fin inner oxide scale (TEM 3 in Figure 9) from sample HRA 8556 (red squared area was mapped).

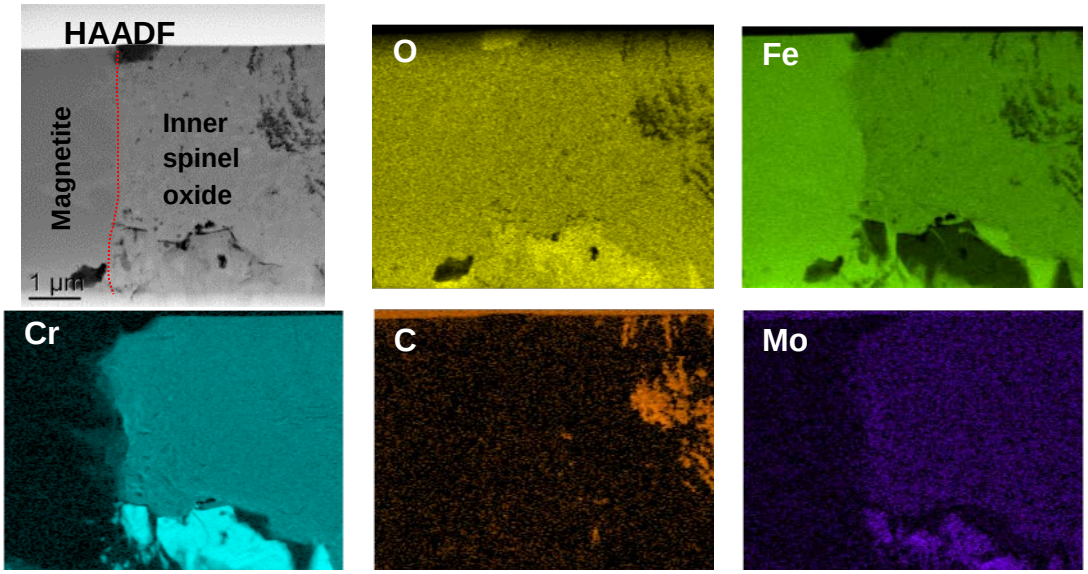

Figure 12 TEM HAADF images with a set of elemental distribution maps collected from the mid fin magnetite/spinel oxide scales interface (TEM 4 in Figure 9) from sample HRA 8556, the magnetite/inner spinel oxides interface is highlighted by the red dash line.

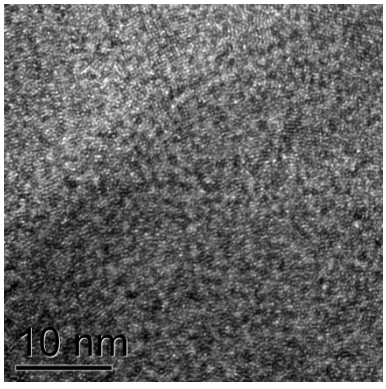

Figure 13 A high-resolution TEM image showing the wavy lattice bands of graphite.

4. Conclusions

Calibrated carbon concentrations were obtained from selected experimental samples after exposure in an autoclave in a simulated service environment. The carbon level was found to peak at the oxide/metal interface and decreased in an approximately linear manner from the interface towards the centre of the sample. The carbon level trend across the fin looks like a ‘V’ shape. Carbon uptake at the oxide/metal interface increased with exposure duration, and eventually approached saturation of carbon across the whole fin.

Carbide particle distributions across the fin were found to be consistent with the carbon content measurements at the same locations. Evenly distributed fine sized particles were observed in the as-received sample; and after exposure in the autoclave, carbides start to coarsen up in size near the metal/oxide interface and gradually across the whole fin. Graphite was observed and identified at the oxide/metal interface of the breakaway fin tip, and also a“tiger mark” of carbon segregation was also found in the inner spinel oxide layer at the location near the magnetite/spinel oxide scale interface.

Acknowledgements:

The authors would like to acknowledge EDF Energy for project funding and J.M. Pearson and A. Shin for technical support on this work.

References

1. P.C. Rowlands, N. Thorne and M.J. Holt, “The Effects of Steel Carbon Content, Gas Pressure and Water Content on the Oxidation of Fe-9%Cr Steels in CO_2”, Central Electricity Research Laboratories, Laboratory Note No. RD/L/N 137/79, July 1079
2. P.C. Rowlands, D.R. Holmes and A. Whittaker; “The Oxidation Behaviour of Fe-9Cr-1Mo Steels”, Gas-Cooled Reactors Today (Vol. 4), (BNES, London, 1983), pp. 173-181
3. P.L. Harrison, R.B. Dooley, S.K. Lister, D.B. Meadowcroft, P.J. Nolan, R.E. Pendlebury, P.L. Surman and M.R. Wootton; “The oxidation of 9Cr 1Mo steels in carbon dioxide A discussion of possible mechanisms”, BNES. International conference on corrosion of steels in CO_2, 1974, pp. 220-233
4. F. Rouillard, G. Moine, L. Martinelli and J.C. Ruiz, “Corrosion of 9Cr steel in CO_2 at intermediate temperature II: mechanism of carburisation”, Oxid Met (2012) 77, pp. 57-70
5. ASTM standard Specification for Seamless Ferritic Alloy-Steel Pip for High-Temperature Service, ASTM International, 2011. A335/A335M-11.
6. S.Yan, S. Davis, S. S. Doak, R. C. Thomson and R. L. Higginson; “Microstructural characterisation of 9Cr 1Mo steel tube”, Loughborough University Phase 3 Final report; NRS/CHEM/BEGL/P(16)191, June 2016
7. G.D. West, Z. Zhou, S. Pickering, M. Brookes, A. Exworthy and S. S. Doak, “Microstructural Characterisation of a 9Cr 1Mo Steel Tube”, phase 2 final report, NRS/CHEM/BEGL/P(13)133, Nov 2013
8. P.C. Rowlands, Corrosion of Steels in CO_2, 1974, pp. 282
9. R.B. Dooley, P.C. Rowlands, M.J. Holt, “A Model for the Breakaway Corrosion of 9%Cr Steels and Alloys in AGR Environments”, CEGB report, RD/L/R 1920, 1975